Mutation Research - Fundamental and Molecular Mechanisms of Mutagenesis 822 (2021) 111743

Contents lists available at ScienceDirect

Mutation Research - Fundamental and Molecular Mechanisms of Mutagenesis

journal homepage: www.elsevier.com/locate/mut

Recruitment of MRE-11 to complex DNA damage is modulated by meiosis-specific chromosome organization

Kailey Harrell, Madison Day, Sarit Smolikove *

Department of Biology, University of Iowa, Iowa City, IA, 52241, USA

ARTICLE INFO

Keywords:
C. elegans
Complex damage/DNA repair
Meiosis
Microirradiation
Synaptonemal complex

ABSTRACT

DNA double-strand breaks (DSBs) are one of the most dangerous assaults on the genome, and yet their natural and programmed production are inherent to life. When DSBs arise close together they are particularly deleterious, and their repair may require an altered form of the DNA damage response. Our understanding of how clustered DSBs are repaired in the germline is unknown. Using laser microirradiation, we examine early events in the repair of clustered DSBs in germ cells within *Caenorhabditis elegans*. We use precise temporal resolution to show how the recruitment of MRE-11 to complex damage is regulated, and that clustered DNA damage can recruit proteins from various repair pathways. Abrogation of non-homologous end joining or COM-1 attenuates the recruitment of MRE-11 through distinct mechanisms. The synaptonemal complex plays both positive and negative regulatory roles in these mutant contexts. These findings indicate that MRE-11 is regulated by modifying its accessibility to chromosomes.

1. Introduction

Clustered DNA double-strand breaks (DSBs) are DSBs found in close proximity to each other [1]. These forms of DNA damage are particularly deleterious as they pose challenges to the DSB repair response. Studies in tissue culture have shown that repair of clustered DSBs involves a shift in DSB repair pathway utilized from non-homologous end joining (NHEJ) to homologous recombination (HR) [2]. Whether a change in repair pathway choice occurs in cells that are already committed to HR is unknown.

One of the tissues most overlooked in studies of repair of clustered DSBs is the germline, a complex tissue that generates gametes through a specialized reductional division termed meiosis. The germline contains a population of stem cells that proliferate mitotically, from which a fraction can differentiate and enter meiosis. Meiotic cells then undergo an extended meiotic prophase I in which programmed meiotic DSBs are induced by the topoisomerase-like protein Spo11 [3]. These DSBs are essential for meiosis because they are required for the formation of crossovers between homologous chromosomes that are in turn essential for their proper segregation into gametes. Meiotic DSBs are committed to repair through HR with a homolog by associating pairs of homologous chromosomes via the synaptonemal complex (SC) [4,5]. In addition to meiotic DSBs, the germline, like any other tissue, is exposed to other forms of DNA damage. This damage can be created by endogenous factors (such as collapsed replication forks) or exogenous factors (such as ionizing radiation). The repair of such damage has potential to be different than the repair of Spo11-induced breaks. One major difference between the types of breaks is the structure of the DSB ends. Spo11 generates breaks by covalently attaching to the DNA and can only be removed by the Mre11-Rad50-Xrs2/Nbs1 (MRX/N) complex [6]. Breaks that do not contain adducts can progress to HR without requiring MRX/N activity [7]. Another difference between exogenously induced and programmed DSBs is in the timing of DSB formation. While meiotic DSBs form only at the entry to meiotic prophase, DSBs formed by radiation can occur at any stage of meiosis or mitosis. Thus, these two types of breaks may experience different repair environments.

The HR pathway is initiated by resection, the processing of DSBs to create single-stranded DNA (ssDNA). Resection is performed by nucleases including the MRX/N complex with its accessory factor Sae2/CtIP/Com-1 [8,9]. The ssDNA is then bound by the RPA complex, which is then replaced by Rad51 which initiates strand invasion, a key step in HR [10]. The covalent binding of Spo11 precludes other repair pathways from operating on these DSBs since ends bound by Spo11 cannot be ligated, and removal requires resection [11]. The ssDNA formed by resection is compatible with HR, but not with NHEJ, an error-prone repair pathway associated with indels and rearrangements [12–15]. In

* Corresponding author.
E-mail address: sarit-smolikove@uiowa.edu (S. Smolikove).

https://doi.org/10.1016/j.mrfmmm.2021.111743
Received 3 December 2020; Received in revised form 11 February 2021; Accepted 15 April 2021
Available online 20 April 2021

mammalian meiotic cells and in yeast meiosis, NHEJ is also inhibited by the downregulation of its components inside of meiotic nuclei [16–18]. Nonetheless, it has been shown in some organisms that NHEJ can act at meiotic DSBs when HR is abrogated, indicating that NHEJ is not necessarily non-functional during meiosis [19,20]. While the presence of a covalently-bound protein drives repair towards HR with programmed meiotic DSBs, it is unclear how regulation of repair pathways occurs at sites of exogenous damage in a meiotic context. Only one study so far has addressed the effect of clustered DSBs in the germline [21]. This study showed evidence for activation of the HR pathway, but the involvement of NHEJ was not examined.

Studies of clustered DNA damage have been focused on generating DNA damage using methods such as high LET and laser microirradiation. The readouts for repair pathway engagement are frequently indirect, by recruitment of DSB repair proteins to the site of damage [22–24]. The type of damage induced by microirradiation universally includes clustered nicks that are formed in close proximity, thus creating clustered DSBs [25,26]. Laser microirradiation has been used primarily in tissue culture, but recently this method was applied to the multicellular organism *Caenorhabditis elegans* [21]. This offers a unique opportunity to study clustered DSBs within the germline of a whole, live organism.

The essential and early role MRE-11 plays in meiotic DSB repair makes it a key site of regulation for DSB repair pathway choice in the germline. As such, we set out to identify how the recruitment kinetics of MRE-11 protein are regulated in vivo. We hypothesized that competing pathways, accessory proteins and meiosis-specific chromosomal structure, will all play a role in the ability of MRE-11 to access DSB repair sites. Here we show that microirradiation induces consistent damage that leads to MRE-11 recruitment as early as 10 s following microirradiation. MRE-11 forms few foci and clusters, the latter composed of multiple, proximal repair sites. Surprisingly these wild-type germ cells recruit a key NHEJ protein that colocalizes with HR factors. We show that cKU-70 does not affect the recruitment time of MRE-11 but influences the formation of clusters in mitotic and early meiotic zones of the germline. In our investigation into accessory factors of the MRN complex, we demonstrate that COM-1 enhances both the recruitment and the activity of MRE-11 at sites of complex DNA damage in the context of a fully formed SC.

2. Materials and methods

2.1. Strains used

Worms were grown and maintained on nematode growth media (NGM) plates that were seeded with *Escherichia coli* OP50. Plates were kept at 20 °C. All strains used were in the N2 (wild type) genetic background. The following strains were used:

N2 (wild type)

mre-11(iow45[mre-11::gfp::3xflag]) V

cku-70(tm1524) III; *mre-11 (iow45[mre-11::gfp::3xflag]) V*

cku-80(iow75[FLAG::cku-80]) III; *mre-11(iow95[mre-11::OLLAS]) V*

com-1(iow101)III/hT2[qls48](I;III); *mre-11(iow45[mre-11::gfp::3xflag]) V*

syp-3(ok758)/hT2 [qls48] I; com-1(iow101)/hT2 [qls48]III; *mre-11 (iow45[mre-11::gfp::3xflag]) V*

syp-3(ok758)I/hT2[qls48](I;III); mre-11(iow45[mre-11::gfp::3xflag]) V

com-1(iow101)/qC1[dpy-19(e1259) glp-1(q339) qls26] III; mre-11 (iow45[mre-11::gfp::3xflag]) V

com-1(iow101)/qC1[dpy-19(e1259) glp-1(q339) qls26] III; him-3 (gk149)/nT1[qls51](IV); mre-11(iow45[mre-11::gfp::3xflag])V/nT1 [qls51] (V)

2.2. Genome editing via CRISPR/Cas9

The following strains were created via CRISPR/Cas9 injections: *mre-11 (iow95[mre-11::OLLAS])* V; *com-1(iow101)/ht2 [qls48]* I;III; *cku-80 (iow75[FLAG::cku-80])* III. Worms were injected as 1-day old adults and recovered onto an NGM plate (for ssODN and crRNA sequences see Table S1). The following day injected worms were singled. Singled plates were then screened for offspring showing *rol* or *dpy* phenotypes associated with mutation of *dpy-10*, the co-injection marker used in each CRISPR injection. *Dpy*, *rol*, and wild type siblings of *dpy/rol* phenotypes were then singled and screened for either an insertion or deletion, depending on injection performed. To verify that the tags did not disrupt the function of the protein we performed functional assays. cKU loss of function has no effect on viability under normal conditions, but late embryos subjected to γ-irradiation show irradiation sensitivity [14]. Eggs were collected from *flag::cku-80* worms and subjected to γ-irradiation to determine sensitivity. Assessment of embryonic lethality and occurrence of abnormal progeny phenotypes revealed no significant difference from wild type (Table S2). Loss of function of *mre-11* leads to almost complete embryonic lethality due to an inability to form or repair DSBs during meiosis [27]. *mre-11::gfp* produced viable progeny indistinguishably from wild type (Table S3). These experiments all together support the functionality of our tags.

2.3. Microirradiation and live imaging

We followed the UV laser microirradiation protocol outlined in Harrell et al. [28] for microirradiation of whole, live worms with the following modifications: for the experiments in all figures except Fig. S1 and Fig. S4, one worm was imaged at a time to allow for 10 s interval acquisition for 15 min without photobleaching. Z stacks of 10 images at 1 μm intervals were taken at each time point. For data presented in Fig. S1, images were taken every 2 min for 1 and a half hours and 2–3 worms were imaged at a time. For data presented in Fig. S4, movies were taken at 40 s intervals for 1 h, and two worms were imaged at a time. For data presented in Figs. 2, 3B, 4, 5, 6EF, 7E-H, S2, S3, and S5 worms were placed on a live-imaging slide, microirradiated, and then recovered. For recovery following microirradiation, 340 μl of M9 was added onto the 10 % agarose pad, allowing worms to be transferred to an NGM plate until dissection or fixation at desired time points. All worms where age matched at the time of microirradiation to be 1 day old adults.

2.4. TrackMate analysis

TrackMate v3.8.0 was used to track foci movement in the live images acquired in MetaMorph version 7.8.12.0 [29]. TIF files were imported into FIJI as 8-bit files with a set scale of 1000 pixels in distance, known distance of 64.5 pixels, pixel aspect ratio of 1, and a unit length of micrometers. The frame was cropped to contain the microirradiated nuclei throughout all frames then hyperstacked. Within TrackMate, the LoG Detector was used with an estimated focus size of 0.6 μm ("blob size" in the program), which corresponds to the threshold of what we consider a small focus versus a cluster (see Results). All movies were blinded and threshold and quality filters for every movie were set to eliminate background. Hyperstack Displayer was used as the viewer. The Simple LAP Tracker was used with the following settings: frame-to-frame linking max distance of 1 μm, max distance of 2 μm, and a maximum frame gap of 5 frames. Filters on tracks were set for each movie to eliminate any background outside of the microirradiated nuclei. Linkage was performed by TrackMate with our parameters listed above and subsequently double-checked with manual corrections when necessary. While connections between foci were manually checked, no additional foci were manually added within these tracks to avoid any bias.

2.5. Intensity measurements

One-day-old adult worms were dissected and transferred to charged slides and kept in the dark as much as possible to avoid photobleaching. The following fixation protocol was used: soaking in -20°C methanol for 1 min, 4% paraformaldehyde (PFA) for 20 min, a 10 min 1xPBST wash, a 10 min 4',6-diamidino-2-phenylindole (DAPI, 1:10,000 of 5 mg/mL stock in 1xPBST) wash, and a 1xPBST wash for 10 min to 1 h. Slides were imaged with MetaMorph version 7.8.12.0 with 100x/1.4 NA oil Leica illuminated with 110LED to capture whole gonad images. Intensity of light source was 5%, with a 500 ms exposure time for both DAPI and GFP channels. 31 images were taken in a stack, with 0.2 μm steps. Measurements of the intensity at the center plane of each nucleus were taken in FIJI in each zone corresponding to where microirradiation is normally performed. The data presented represent the average intensity of that stack and therefore reflect arbitrary units (A.U.) per area. Fluorescence intensity was corrected to cytoplasmic background by subtraction.

2.6. MRE-11::GFP time course analysis

One-day-old adult worms were microirradiated on live-imaging slides in indicated zone (TZ (Fig. 4) or MP (Figure S3)) and then recovered. Ethanol fixation was performed with the following protocol at indicated time points following microirradiation for each worm (as indicated in Results, Fig. 4 and Figure S3): 5–10 adult worms were placed on an uncharged slide (Surgipath Leica) in 5 μl M9 solution, most liquid was soaked up using filter paper, then 5 μl ethanol was applied and allowed to evaporate, followed by application of 5 μl M9-DAPI dilution. Most of this solution was soaked up using filter paper again and a coverslip with Vectashield was placed on top. Coverslips were sealed with acrylic nail polish. Images were taken on the DeltaVision wide-field fluorescence microscope (GE Lifesciences) with 100x/1.4 NA oil Olympus objective. Images were then deconvolved with softWoRx software (Applied Precision). Microirradiation was indicated by the presence of bright green foci, as no foci appear at endogenous DSBs, and these nuclei were scored.

2.7. TUNEL assay

Five 1-day-old adult worms were placed on a live-imaging slide at a time according to the protocol outlined in Harrell et al. [28]. All four germline zones were targeted in both gonads of each worm and microirradiated at 15 % attenuation (as for all microirradiation carried out in this paper). Worms were recovered and both gonads were dissected 15 min post-microirradiation. Apoptosis analysis in wild type worms was carried out on 1-day-old adult worms without application of microirradiation. Terminal deoxynucleotidyl transferase-mediated dUTP nick-end labelling (TUNEL) protocol was followed as described in [30] with the following modification: slides were incubated for 30 min at room temperature in 0.1 M Tris-HCl (pH 7.5) containing 1% BSA and no bovine serum. Imaging was performed on the DeltaVision wide-field fluorescence microscope as listed previously in MRE-11::GFP Time Course Analysis.

Volume of DNA, determined via volume of DAPI staining, was calculated using volume of a sphere equation ($4/3\pi r^3$) with the inner, hollow sphere of the nucleus being subtracted from the outer sphere of DNA to get an accurate measurement of the DAPI volume:

$$\left(\frac{4}{3}\pi r^3\right)_{Outer\ Sphere} - \left(\frac{4}{3}\pi r^3\right)_{Inner\ Sphere}$$

Radius of the sphere was calculated using known step sizes of 0.2 μm between stacks and the top and bottom limits of the DAPI stain, and the area of the sphere was taken at the middle plane of the nucleus.

Volume of the TUNEL stain was determined via volume of a trapezoid, which employs the use of areas of irregular shapes. Each plane of the image was scrolled through for each nucleus and the total area of staining for every plane was calculated. The following formula was applied to determine overall volume:

$$0.1 * (a_1 + 2 * a_2 + 2 * a_3 + \ \ldots . a_n)$$

0.2 μm is the step size, therefore 0.1 is the radius of each plane. a_1 is the area of the first plane of the nucleus with staining, followed by each subsequent plane (a_2 and a_3) until the final plane with staining is reached (a_n).

2.8. Immunostaining

One-day-old worms were microirradiated, recovered, and dissected in M9 solution on a coverslip and transferred onto positively charged slides, then placed onto aluminum blocks in dry ice. Worms were kept in the dark as much as possible throughout this protocol to avoid photobleaching. Antibody staining was performed by the following procedure: wash in -20°C methanol for 1 min, 4% PFA for 30 min, wash in 1xPBST for 10 min, block in 0.5 % BSA in 1xPBST for 1−2 hours, then incubated with the primary antibody overnight at room temperature. Following primary antibody incubation, slides were washed in 1xPBST 1–3 times for 10 min each, then incubated with the secondary antibody for 2 h at room temperature in the dark, followed by 1xPBST wash for 10 min, 10 min staining in DAPI (1:10,000 of 5 mg/mL stock in 1xPBST), and a wash in 1xPBST for 10 min-1 h. All antibodies used were diluted in 1xPBST. For the SYP images presented in Fig. 8A, no microirradiation was performed prior to dissection and staining. Primary antibodies used were: rabbit anti-RAD-51 (1:30,000), mouse anti-FLAG (1:500; Sigma F1804), rabbit anti-OLLAS (1:1,000; Genscript #A01658), goat anti-SYP-1 (1:500), and rabbit anti-HTP-3 (1:500). Secondary antibodies used were: goat anti-rabbit Alexa Fluor 555 (1:500; Invitrogen), donkey anti-rabbit Alexa Fluor 488 (1:500; Thermo), and donkey anti-mouse Cy3 (1:500). Anti-FLAG and RAD-51 were quantified using background reduction as in [31].

2.9. γ-Irradiation

1-day-old adult worms were exposed to 100 Gy of γ-irradiation from a cesium source and dissected 1 h post-irradiation. Worms were then stained according to the immunostaining protocol listed above.

2.10. Statistical analysis

All statistics were performed using GraphPad Prism 8. For all data presented, a normality and logarithmic test was employed on the data to determine if the distribution of the data was normal or not. If all distributions were normal and there were only two groups being compared, a parametric *t*-test was employed. If all distributions were normal and there were more than two groups being compared, an ANOVA was employed to determine which groups had statistically significant differences and then a *t*-test was performed to determine exact p-values for statistical differences. If even one distribution was not normal, and there were only two groups to be compared, Mann-Whitney U-test was performed. If there were more than two groups, Kruskal-Wallis was employed to determine significant differences between rank means. For all pairwise comparisons that presented with a significant difference through this test, Mann-Whitney U-test was performed to determine an exact p-value.

3. Results

3.1. MRE-11 exhibits recruitment kinetics to microirradiation-induced breaks consistent with its role in meiosis

To study early events of DNA repair at complex DSBs in vivo, we used UV laser microirradiation to generate DSBs in individual germline nuclei

of live *C. elegans* without increasing apoptosis or damaging adjacent germline nuclei that were not microirradiated [21]. Our previous studies were done in the *spo-11* mutant background. To test if HR proteins localize to microirradiation-induced breaks and form clusters of DSBs in wild-type nuclei we followed MRE-11, a member of the MRN complex and the major nuclease that processes meiotic DSBs [32,33]. Consistent with its role in formation and processing of meiotic DSBs, MRE-11 is found in all germline nuclei (as evidenced by its concentrated nuclear haze) but does not form foci (Fig. 1A (left image) and Fig. 1B) [34]. MRE-11's mechanism of action suggests that it can be used as an early marker for DSB repair following DSB cluster formation in meiosis, as found in mammalian (mitotic) tissue culture studies [35,36].

We have shown previously that MRE-11::GFP is expressed in all germline nuclei [34]. Since MRE-11 recruitment to microirradiation-induced breaks may be influenced by its relative nuclear concentration, we determined if the amount of MRE-11 protein localizing to nuclei is altered throughout the germline. We measured the fluorescence intensity of MRE-11::GFP throughout four regions of the germline examined in this study: pre-meiotic tip (PMT), transition zone (TZ), mid-pachytene (MP), and late-pachytene (LP). In the *C. elegans* germline, nuclei divide in the PMT (most are in S/G2) and are pushed to move toward the uterus. As they move, they enter meiotic prophase I (in the TZ) and progress through all the stages of meiotic prophase I, including MP and LP, in consecutive order. Thus, in a single germline ~1000 nuclei are found organized in a temporo-spatial order. The intensity of MRE-11::GFP expression significantly increases with progression through the germline (Fig. 1B and S1A). This increase in expression is consistent with MRE-11's transition from a redundant role (mitosis) to an obligatory role (meiosis) in the repair of DSBs in the germline and may also reflect protein accumulation for ensuring sufficient MRE-11 levels in the embryo.

To study MRE-11 recruitment to microirradiation-induced damage we had to determine the conditions of the live-imaging experiments (frames/minute) which affects the overall time of imaging. Acquiring live-imaging data is limited by photobleaching, thus longer imaging times allows later appearing foci to be detected, but needs to be performed at a lower resolution (less frames/minute). This prevents the detection of foci undergoing fast turnover and over-estimates time of appearance (i.e., foci appearing 10 s post-microirradiation will be recorded as appearing at 2 min, when acquisition is done every 2 min). Thus the conditions of live-imaging experiments have tradeoffs, and results of the analyses performed is relative to the experimental conditions. Here, we conducted live-imaging experiments in a 15-minute window following microirradiation based on the rationale presented below. We previously demonstrated that upon microirradiation, RPA-1 and RAD-51 form foci at sites of damage ~8 and ~20 min post-microirradiation, respectively [21]. First, since RPA-1 binds ssDNA, RPA-1 focus formation is dependent on DNA resection. Therefore it is expected that MRE-11, the nuclease forming ssDNA, will be recruited to DSBs prior to RPA-1, suggesting that a time window of 15 min will be

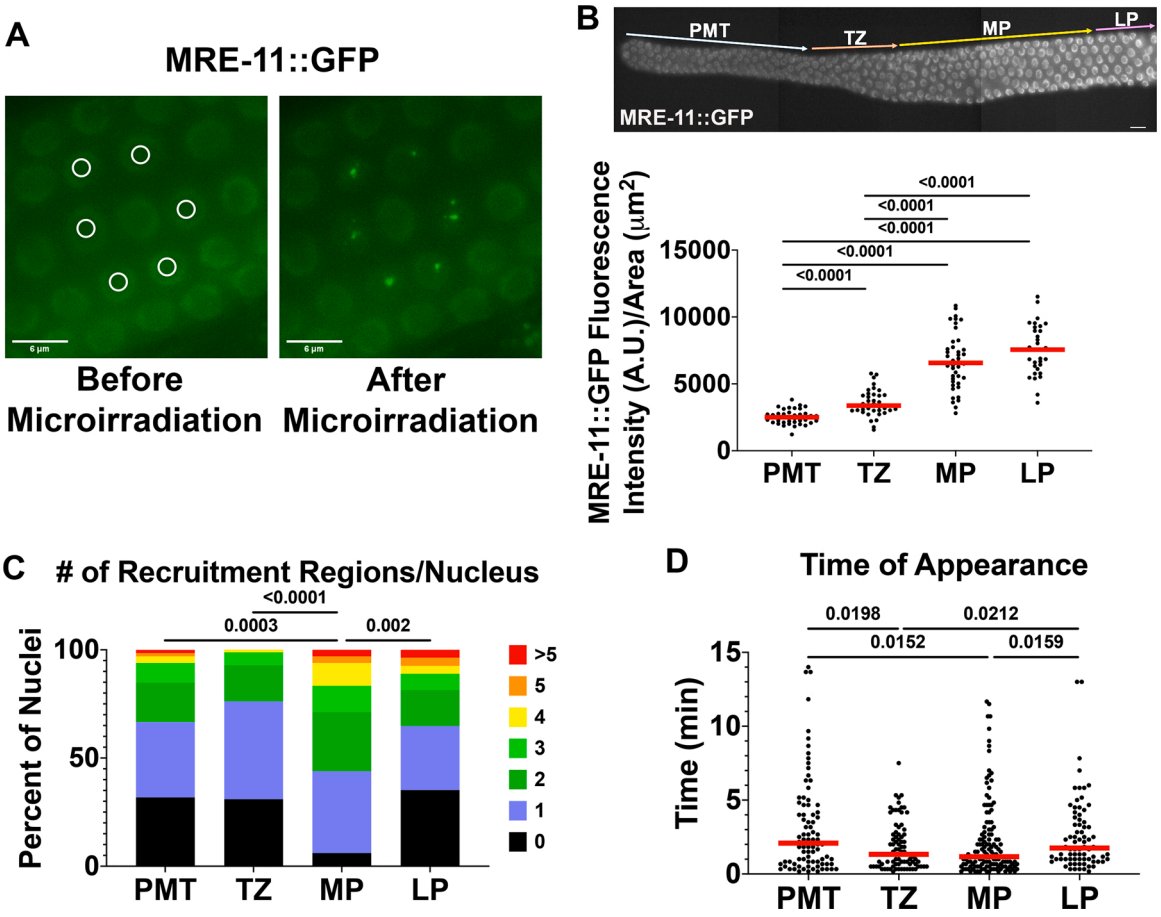

Fig. 1. MRE-11 is recruited to microirradiation-induced DNA damage within the *C. elegans* germline. A) Example of microirradiation-induced foci in the *mre-11::gfp* strain. Left panel is MP nuclei before microirradiation, right panel is MP nuclei 4 min post-microirradiation. White circles in left panel indicate targeted nuclei. B) Top: A dissected gonad from an *mre-11::gfp* worm. Scale bar =10 μm. Bottom: Fluorescence intensity of MRE-11::GFP per area in the four main germline zones studied in this paper. Horizontal red line indicates median. Each point is an individual nucleus. Values were corrected to cytoplasmic background. C) Number of recruitment regions per nucleus after microirradiation. D) Time of recruitment region appearance in minutes after microirradiation. Each data point represents an individual region. Horizontal red lines indicate median. For data sets with more than 2 groups (B, C, and D) Kruskal-Wallis was applied to determine significant differences between rank means, and if there was determination of significant differences, Mann-Whitney U-test was applied for each pairwise comparison.

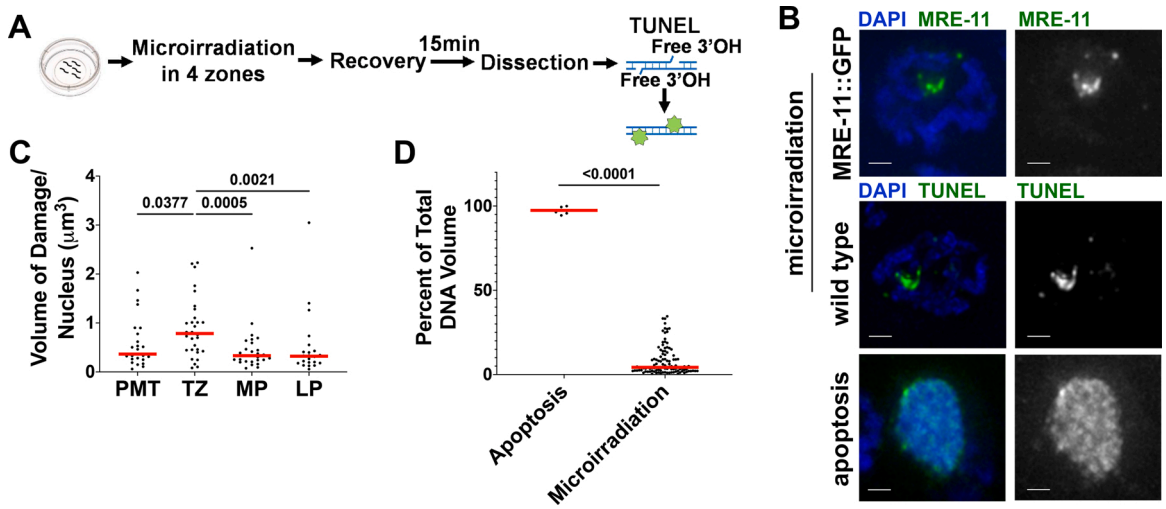

Fig. 2. Microirradiation induces damage that is distinct from apoptotic levels of damage. A) Experimental design for the terminal deoxynucleotidyl transferase dUTP nick end labeling (TUNEL) assay. B) Examples of nuclei that were hit with microirradiation (top two rows) or are apoptotic (bottom row). The top row is an example of MRE-11::GFP seen after microirradiation in MP (no staining). The middle row is from a wild-type worm and is an example of TUNEL staining in an MP microirradiated nucleus. The bottom row is TUNEL staining of an apoptotic nucleus in LP in a wild-type worm. Scale bars =1 μm. C) Volume of damage per nucleus that is marked by TUNEL staining after microirradiation in each germline zone. D) Percent of total DNA volume that is marked by TUNEL staining. The apoptosis column includes data from apoptotic nuclei in LP while the microirradiation column contains data from microirradiated nuclei in PMT, TZ, MP, and LP. Mann-Whitney U-test used to assess significance. Kruskal-Wallis was applied to determine significant differences between rank means (C). Mann-Whitney U-test was applied for each pairwise comparison (C and D). Horizontal red lines on graphs in C and D indicate median.

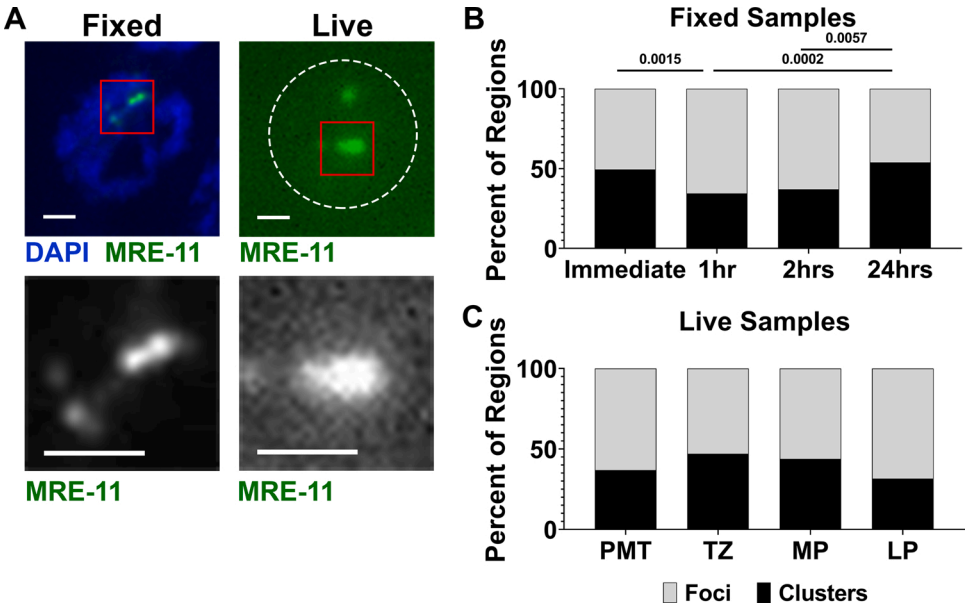

Fig. 3. Clusters are made up of 2+ foci and can be resolved into individual foci in fixed images. A) Examples of clusters and foci in microirradiated nuclei that were fixed (left) or live imaged MRE-11::GFP worms. Dotted white line is the nuclear outline in the right panel. Red square in each panel is the area that is in the close-up panel below. Scale bar =1 μm. B) Percent of total regions of DNA damage that are either foci or clusters in the fixed imaging. C) Percentage of microirradiation-induced recruitment regions that are clusters (>0.6 μm, black) or foci (≤0.6 μm, gray) in the analyzed live imaging. Fisher's Exact Test (two-tailed) was applied for all pairwise comparisons in B and C.

most appropriate for imaging MRE-11. Second, 15 min of total imaging permits data acquisition every 10 s, which allows high resolution timing of focus formation (67 % of foci appear in the first 2 min, Fig. S1B) and allows the detection of MRE-11 foci with a duration of less than 2 min (15 % of the foci). The only disadvantage of 15-minute imaging is that foci formed at later time points will not be detected (24 % of foci, Fig. S1C). To improve upon our data analysis utilized in the protocol from Koury et al., 2018, we use an automated focus calling software (for details see Materials and Methods [29]). We examined recruitment kinetics of MRE-11 by 3D imaging every 10 s following microirradiation for 15 min to obtain a live time-course of MRE-11 recruitment (Fig. 1, Movie S1). Worms were microirradiated in 4 germline zones: PMT, TZ, MP, and LP. Images were analyzed using the FIJI Plug-In TrackMate to obtain number of foci per nucleus and the time of focus recruitment (see Materials and Methods).

We found that MRE-11 forms significantly more foci in MP compared to all other germline zones (average 2 foci/nucleus vs. 1 focus/nucleus; Fig. 1C), similar to what we observed for RAD-51 [21]. Another measurement for recruitment of MRE-11 to DSBs is the time it takes for a focus to appear. Although a similar number of sites may be eventually available for MRE-11, the speed by which a focus forms can vary. This could be indicative of the ability of MRE-11 to access damage sites. MRE-11 is recruited to microirradiation-induced breaks ~2 min on average post-microirradiation in TZ and MP (early meiosis), which is significantly faster than the ~3 min it takes for focus formation in PMT and LP (Fig. 1D). The acquisition of RPA-1 recruitment time in [21] was done using different parameters (2-minute intervals). To directly compare recruitment of MRE-11 to RPA-1, we also analyzed MRE-11 at

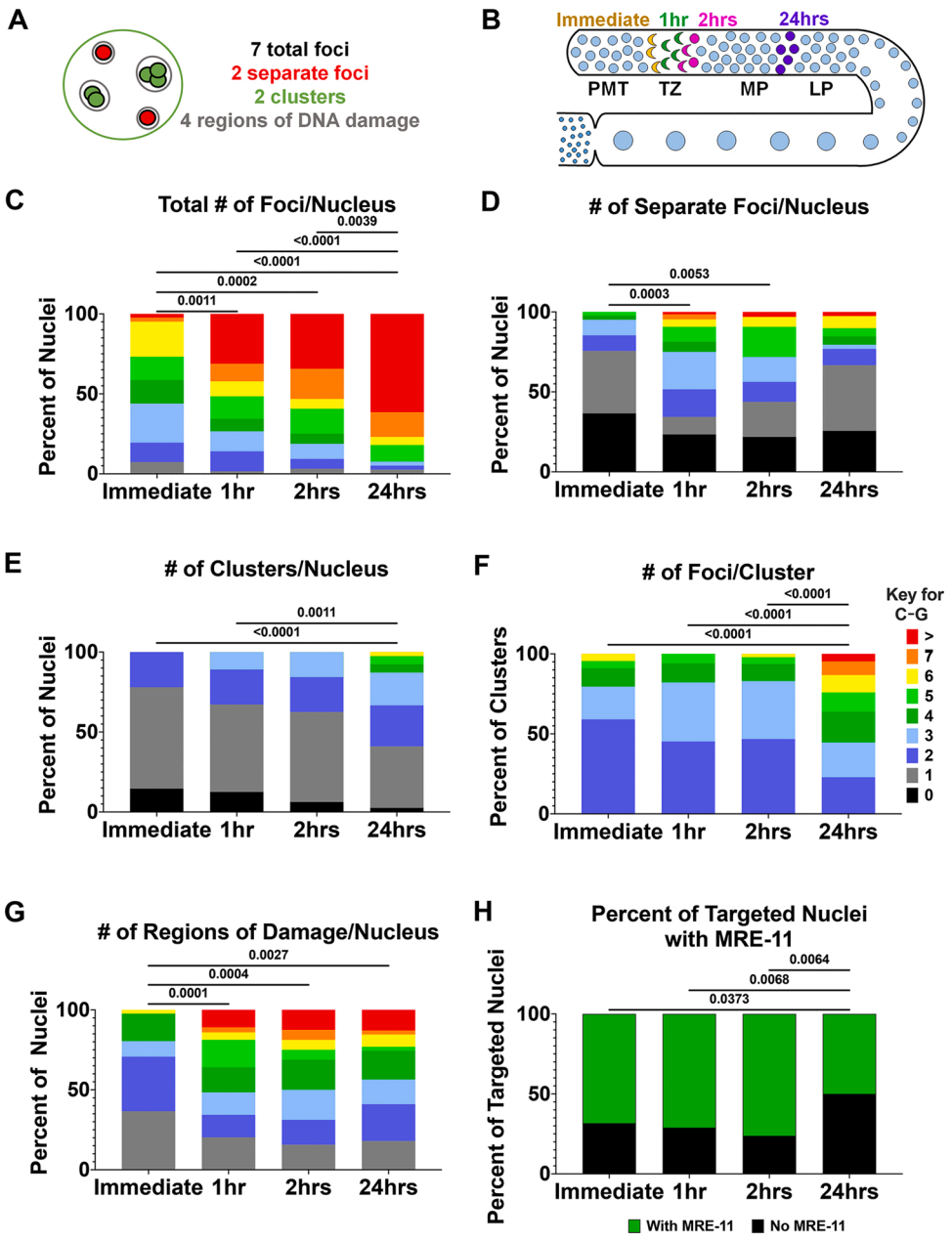

Fig. 4. MRE-11 exhibits an increase in foci and clusters in a 24 -h time period following microirradiation. A) Cartoon depicting the terminology for classifying the microirradiation-induced damage in fixed samples. "Total foci" is the total number of foci in the nucleus (outlined in black). "Separate foci" are foci that are not touching any other foci (red). "Clusters" are 2 or more foci that are touching (green). "Regions of DNA damage" is the number of clusters and separate foci within the nucleus (outlined in gray). B) Schematic of the *C. elegans* germline. Worms are microirradiated in TZ and then EtOH fixed at indicated time points: Immediate (12 min), 1 h, 2 h, or 24 h. Each time point is marked with a distinct color in the germline cartoon and indicates where the nuclei are in the germline upon fixation at that time point. Legend to the right of panel F applies to C-G. C) Total number of foci (within clusters and separate foci) per nucleus. D) Number of separate foci per nucleus. E) Number of clusters per nucleus. F) Number of foci per cluster. G) Number of regions of DNA damage per nucleus. H) Percent of nuclei targeted with microirradiation that have MRE-11 regions of damage at each time point. For data sets with more than 2 groups (C-G) Kruskal-Wallis was applied to determine significant differences between rank means, and if there was determination of significant differences Mann-Whitney U-test was applied for each pairwise comparison. For H, Fisher's Exact Test was used for all pair-wise comparisons.

MP using 2-minute interval movies and the same focus size calling as in [21]. By this analysis, MRE-11 appeared ~4 min earlier than RPA-1 (Fig. S1D). The time of recruitment is consistent with our previous data and the role of MRE-11 in generating ssDNA for recruitment of RPA-1 and RAD-51, both of which show average recruitment times longer than that of MRE-11. Altogether, this indicates that the ability of MRE-11 to be recruited to DSBs is different throughout the germline, and this difference may reflect regulation of its activity.

3.2. *Microirradiation induces similar levels of localized damage throughout the germline*

We assume that the number of MRE-11 foci reflects the ability of MRE-11 to access the location of damaged DNA. However, this acts under the assumption that the same DNA damage was formed in each germline region tested. Since we used exactly the same laser power throughout the worm and all germline regions are positioned roughly the same distance from the laser and the edge of the worm's body, we did not expect any differences in level of damage inflicted. To test this, we employed the terminal deoxynucleotidyl transferase-mediated dUTP nick-end labelling (TUNEL) assay which marks free 3′-OH and in doing so marks DNA damage (Fig. 2A). The protocol utilized does not mark SPO-11 induced breaks, likely due to interference from DSB binding and processing proteins. TUNEL is the most direct measurement of DNA damage created by laser microirradiation, as the mechanism of action of microirradiation is the formation of DNA nicks and, when clustered, nicks form DSBs [25]. Immediately following microirradiation, germlines exhibited localized TUNEL signal that was never found in non-microirradiated germlines (Fig. 2B, second row). The number of affected nuclei is consistent with DNA damage specific to microirradiated nuclei (Fig. S2A).

Apoptosis also results in TUNEL-positive nuclei due to fragmentation of chromosomes that is part of the apoptotic process which is restricted to LP. However, this type of DNA damage is not localized and affects all nuclear DNA [37]. To determine if microirradiation-induced DNA damage is distinct from that formed by apoptosis, the area of all stained

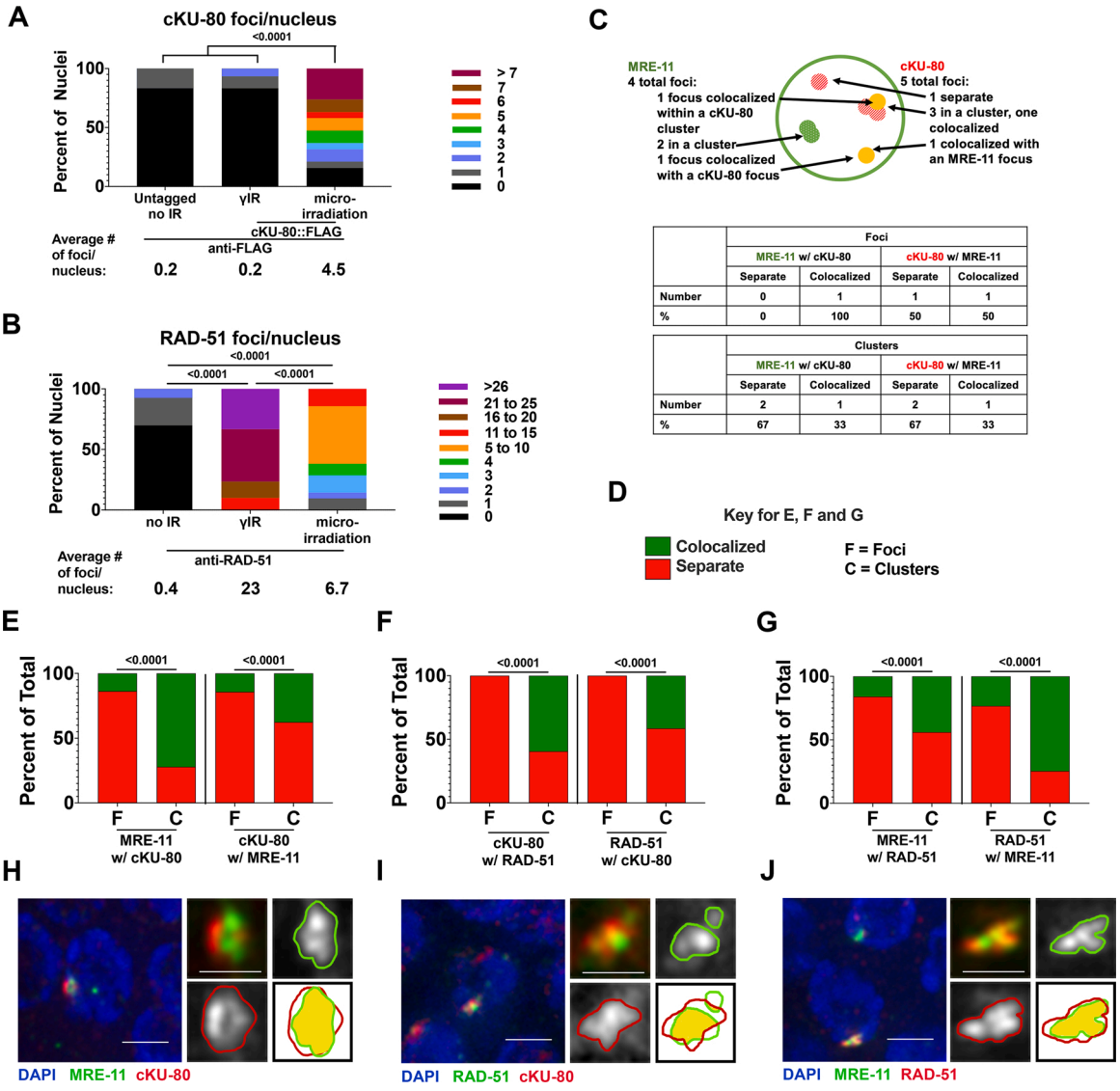

Fig. 5. NHEJ proteins are not recruited to γ-irradiation-induced damage and DNA repair factors colocalize in clusters more often than as foci 1 h following microirradiation in TZ. A) Percentage of nuclei with the indicated number of cKU-80 foci per nucleus in an untagged strain without irradiation (N2) and in a tagged strain (FLAG::cKU-80) with either γ-irradiation (γIR) or microirradiation. Numbers below each condition indicate average number of foci per nucleus. B) Percentage of nuclei with the indicated number of RAD-51 foci per nucleus with no irradiation (no IR), with γ-irradiation (γIR) or with microirradiation. Numbers below each condition indicate average number of foci per nucleus. C) a cartoon representing how the data in this figure is analyzed with a specific example in the tables below the cartoon. Labels for the graphs presented in E-G for classification of colocalization are: separate indicates no overlap or touching (red), colocalized indicates overlap (green). D) Key for E-G. E) Colocalization data for MRE-11 and cKU-80 marked with anti-OLLAS and anti-FLAG antibodies, respectively (*mre-11::ollas; flag::cku-80* strain) This represents colocalization for microirradiation-induced damage split into foci and clusters for either MRE-11 with cKU-80 or for cKU-80 with MRE-11. F) Colocalization data for cKU-80 and RAD-51 marked with anti-FLAG and anti-RAD-51 antibodies, respectively (*mre-11::ollas; flag::cku-80* strain). This represents colocalization for microirradiation-induced damage split into foci and clusters for either cKU-80 with RAD-51 or for RAD-51 with cKU-80. G) Colocalization data for MRE-11 and RAD-51 marked with GFP and an antibody against RAD-51, respectively (*mre-11::gfp* strain). This represents colocalization for microirradiation-induced damage split into foci and clusters for either MRE-11 with RAD-51 or for RAD-51 with MRE-11. H-J) Representative images of microirradiated nuclei after dissection and staining for indicated proteins. Scale bars =3 μm.The grid of four images to the right of each large representative image is a zoomed in view of a cluster. Top left image in the grid is the two channels merged, top right is the green channel (MRE-11 in H and J, RAD-51 in I), bottom left is the red channel (cKU-80 in H and I, RAD-51 in J), and the bottom right image is an overlap of the tracings down in the individual channels. Yellow indicates what would be considered colocalized. Scale bars in the close-ups =1 μm. For B and C a Mann-Whitney U-test was performed for all pairwise comparisons. For statistics in E-G, a Fisher's Exact Test was performed between the Separate and the Colocalized category.

regions through the image stack was taken and volume was calculated for each nucleus (Fig. 2C and S2B). The volume was then normalized to DAPI to indicate the percent of DNA that contains 3'-OH DNA (Fig. 2D and S2CD). Only ~8% of the DNA volume of microirradiated nuclei stained with TUNEL, compared to 97 % of apoptotic nuclei (Fig. 2D). This clearly indicates that the DNA damage following microirradiation is localized and distinctly different from apoptotic DNA damage.

Moreover, comparing the amount of damage between zones (total area of TUNEL, Fig. 2C) staining per nucleus indicated that the damage induced in each germline zone was similar. The organization of chromatin changes as nuclei progress into and through meiosis which is reflected in an increase in DAPI volume (Fig. S2B), leading to a decrease in the relative area of TUNEL staining in MP and LP compared to other stages (Fig. S2D). The percent of nuclei with TUNEL staining out of nuclei irradiated was consistent throughout the germline (Fig. S2A). Overall, this indicates that the damage induced in all of our studied

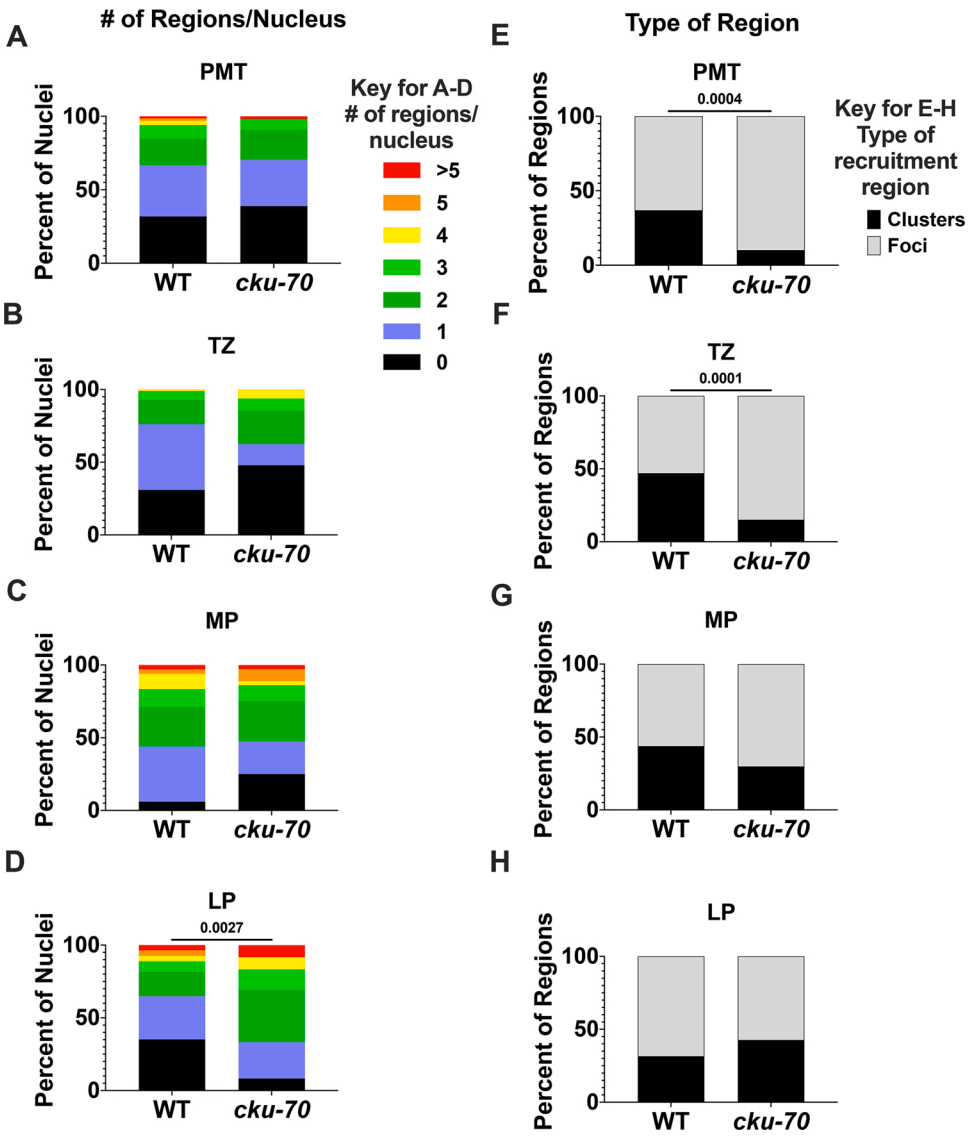

Fig. 6. Deletion of cKU-70 leads to differential MRE-11 focus formation after microirradiation in PMT and TZ. *cku-70(tm1524)* mutant allele used for *cku-70* mutant in this Figure. A-D) The percentage of nuclei with the indicated number of recruitment regions in each germline zone. Figure legend in A applies to graphs in A-D. E-H) The percentage of clusters (>0.6 μm, black) versus foci (≤0.6 μm, gray) in each microirradiated zone. Figure legend in E applies to E-H. For A-D Mann-Whitney U-test was employed. For E-H Fisher's Exact Test (two-tailed) was used.

germline regions was similar, localized, and not confounded by location within a whole worm. Most importantly, MP and LP were exposed to identical damage (Fig. 2 and S2) and showed identical MRE-11 protein expression (Fig. 1B), indicating that the differences observed between these stages in their ability to recruit MRE-11 reflects a biological difference in MRE-11's ability to access breaks.

3.3. MRE-11 forms two types of focus configurations: individual foci and clusters

In our previous studies using fixed samples we noted that following microirradiation RAD-51 forms both individual foci and foci clusters (2 or more foci that are touching [21]). The size of foci in the "individual foci" category was identical to that of RAD-51 foci induced by SPO-11 that are considered sites in which a single DSB is formed (Fig. S2E). This suggests microirradiation creates two classes of damage sites: ones that contain multiple events (clusters) and ones that likely contain individual events (individual foci). Analysis of fixed samples from MRE-11::GFP retrieved at different time points post-microirradiation (see below) was consistent with this observation (Fig. 3A), indicating that both complex (clusters, 2 or more foci touching each other) and less complex (single focus) DNA damage is formed following microirradiation. These events were evenly split in proportion (Fig. 3B) with minor differences between zones. The resolution of the images obtained from live-imaging analysis does not allow detection of individual foci within a cluster (Fig. 3A). However, such discrimination can be done by examining the size of the focus. We used the average diameter of the clusters defined by fixed sample analysis to divide the categories of damage observed by live imaging into clusters and foci (Fig. 3A). Based on this analysis, we set the threshold to identify foci in the time course images as 0.6 μm and we used this threshold to distinguish between foci (≤0.6 μm) and clusters (>0.6 μm). The ratio of these foci and clusters was then examined in each of the four zones microirradiated. This form of analysis yielded similar results to that obtained by fixed sample analysis: around 50 % of damage regions formed upon microirradiation were clusters, and there was no significant difference between the four zones regarding ratio of clusters to foci (Fig. 3C). Thus, our method of assigning foci versus cluster categories for live-imaged foci likely reflects foci and clusters identified by immunofluorescence analysis. All together this data shows that microirradiation creates two types of DNA damage sites that vary in the amount of DNA damage. To refer to clusters and foci collectively we will use the terminology "recruitment regions". The presence of clusters allows us to test the hypothesis that clustered breaks are repaired using different mechanisms compared to foci that are not in clusters.

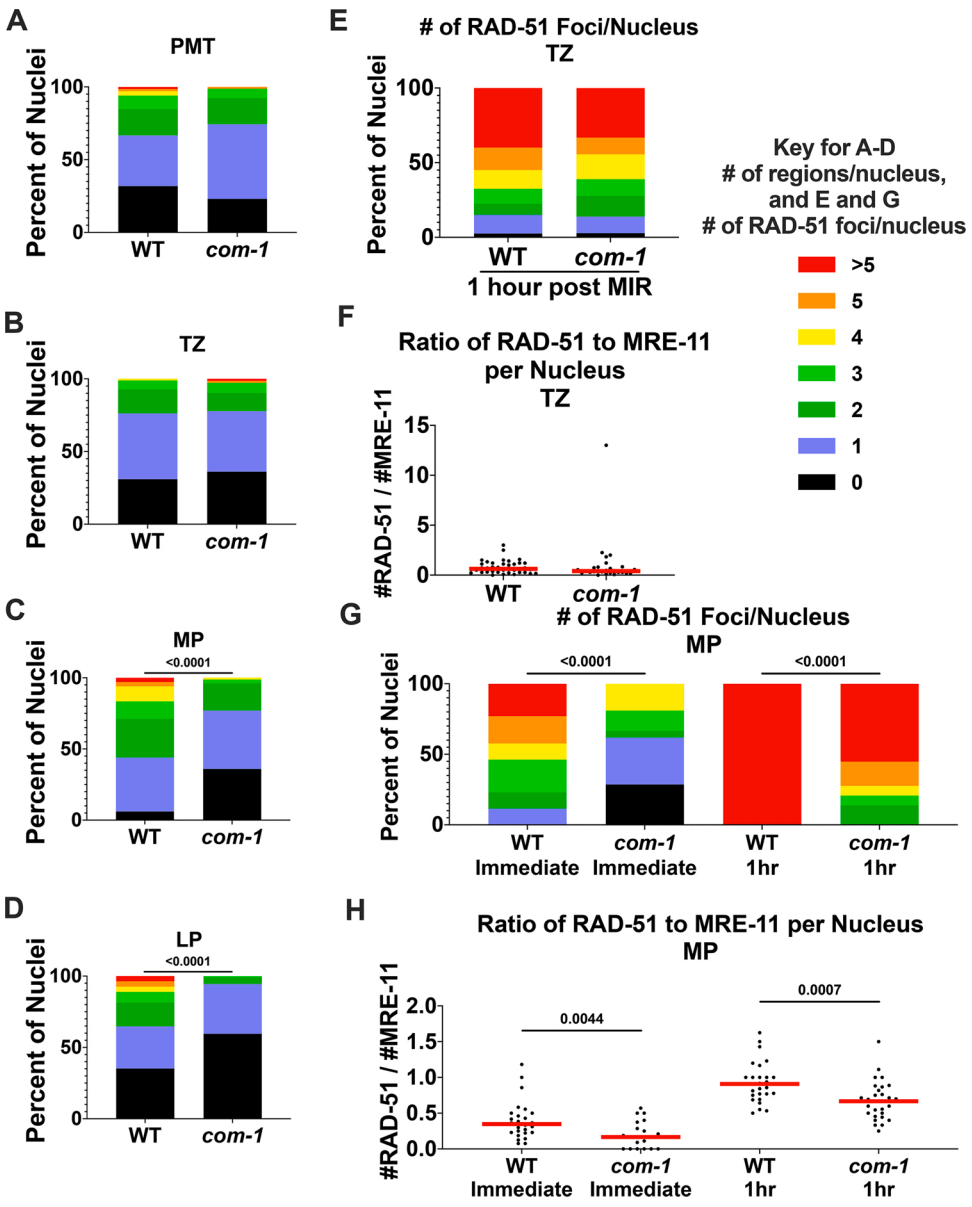

Fig. 7. Deletion of COM-1 decreases MRE-11 recruitment and resection activity in MP and LP. *com-1(iow101)* mutant allele used in this figure for *com-1* mutant. A-D) Percentage of nuclei with the indicated number of recruitment regions. E) Percentage of nuclei with the indicated number of RAD-51 foci in nuclei microirradiated in TZ, recovered, and dissected 1 h post-microirradiation. F) The ratio of RAD-51 to MRE-11 foci within nuclei quantified in E, with the number of RAD-51 foci per nucleus divided by the number of MRE-11 foci within the same nucleus. G and H) Worms were microirradiated in MP, recovered, and dissected either immediately or 1 h later. G) Percentage of nuclei with the indicated number of RAD-51 foci per nucleus. H) The ratio of RAD-51 to MRE-11 foci within nuclei quantified in G, with the number of RAD-51 foci per nucleus divided by the number of MRE-11 foci within the same nucleus. Each data point represents a single microirradiated nucleus. Horizontal red bar indicates the median in graphs in panels F and H. For A-D Mann-Whitney U-test was employed. For E-H Mann-Whitney U-test was used for statistical comparison between wild type and *com-1* mutants at both time points.

3.4. MRE-11 shows an increase in recruitment over a 24 -h time period

Germline DSB repair occurs over the course of hours for both SPO-11-induced DSBs and microirradiation-induced DNA damage [21,38]. However, worms can endure live-imaging for no more than a couple of hours (typically one hour), which precludes the analysis of the whole process of DSB repair by live-imaging. To gain a better understanding of the duration and kinetics of repair of clustered DSBs in wild-type nuclei, we performed microirradiation, recovery, and gonad fixation at varying time points on our MRE-11::GFP strain. The drawback of this method is first, that the most immediate time point in which such analysis can be performed is 12 min following microirradiation, precluding analysis of early events of recruitment that live-imaging permits. Second, only nuclei with an MRE-11 focus or foci could be followed. The advantage of fixed sample analysis is two-fold. First, it provides the ability to look at the repair process hours and even days after DNA damage induction. Second, it can provide more detailed information, as single foci can be resolved both separately (Fig. 4A, red) and within clusters (2 or more foci touching, Fig. 4A, green). Thus, the number of foci per cluster and the total number of foci in a nucleus can be determined (Fig. 4A, black). When a cluster and a separate focus are each classified as a single "region" of DNA damage (Fig. 4A, gray) that provides a metric for comparison with our live-imaging data ("recruitment regions").

Microirradiation was performed in TZ, the region in which programmed meiotic DSBs are typically formed. Four time-points post-microirradiation were examined: immediate (12 min), 1, 2, and 24 h post-microirradiation. Nuclei move in the germline at a rate of about 1 nucleus row per hour, thus the process of DSB repair occurs concurrently with progression through meiosis. The position of nuclei post-microirradiation was consistent with their rate of movement in the absence of microirradiation; at the immediate and 1 h time points, nuclei were still in TZ at the time of fixation, while nuclei examined at the 2 h time point were in TZ transitioning to EP and nuclei at the 24 h time point were either in MP or LP (Fig. 4B).

MRE-11 shows a significant increase in the total number of foci per nucleus (this includes both separate foci and all foci present in clusters) over the time course analyzed (Fig. 4C, ~4, 6, 7 and 11 foci per nucleus at the immediate 1, 2 and 24 h timepoints post-microirradiation respectively). We then broke down the numbers of total foci per nucleus to assess whether separate foci or foci in clusters were contributing to this increase in the total number of foci. The number of separate foci per nucleus increased significantly between the immediate and 1 -h time

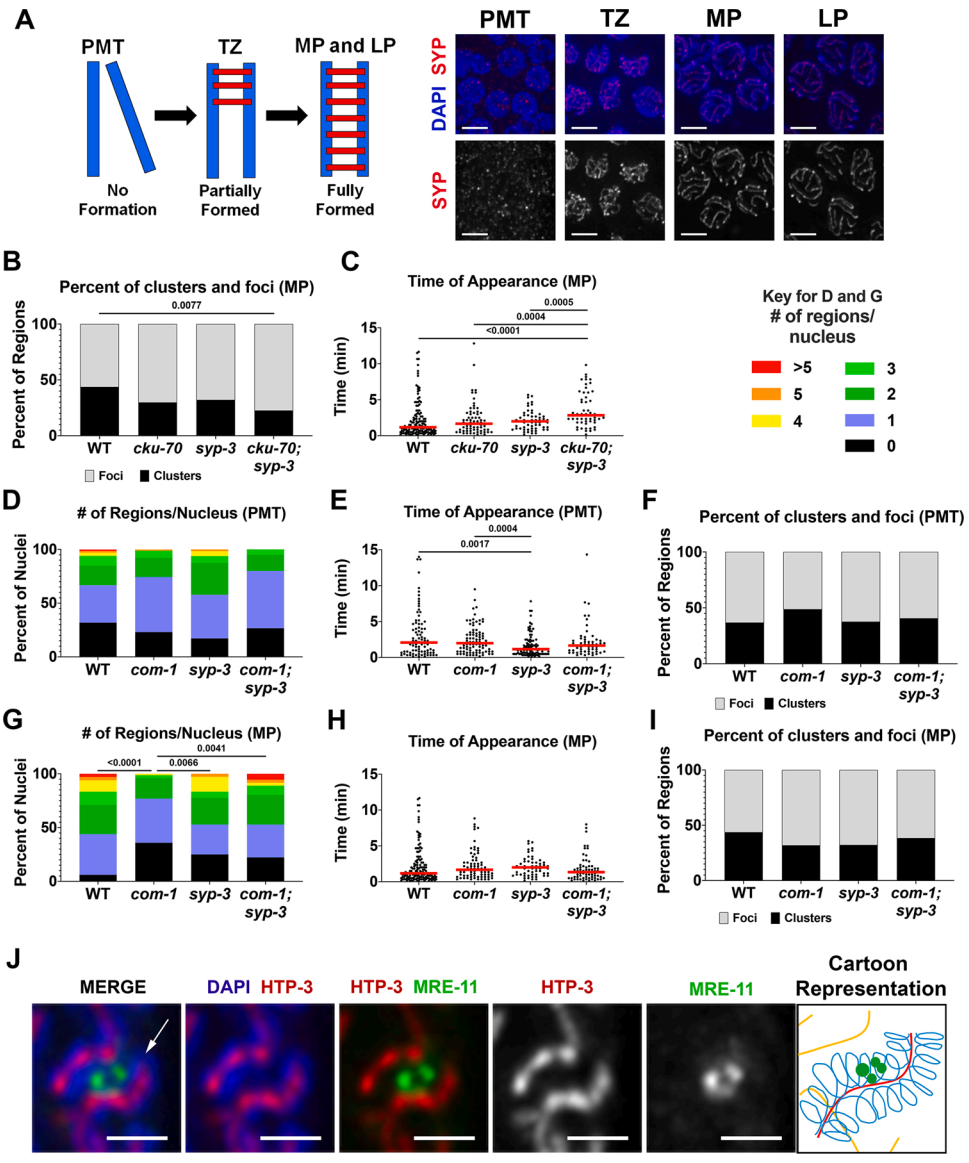

Fig. 8. COM-1 and KU are required for normal recruitment kinetics of MRE-11 in the presence of the synaptonemal complex. *syp-3(ok758)* mutant allele used in this Figure. A) Progression of the formation of the synaptonemal complex (SC). In TZ synapsis is initiated, by MP the SC is fully formed, and at the end of LP there is partial disassembly of the SC. Blue bars in the cartoon represent homologous chromosomes and the red is the proteinaceous SC which forms between them. On the right are representative images of each germline zone with SYP-1 staining shown in red. Scale bar =3 μm. B) Percentage of regions that are either clusters (>0.6 μm, black) or foci (≤0.6 μm, gray) after microirradiation in MP. C) Time of appearance of regions of recruitment in minutes after microirradiation in MP. Each data point represents a single region. Horizontal red bar indicates median. D) Number of recruitment regions per nucleus in PMT. E) Time of focus appearance (minutes) in microirradiated nuclei of PMT. Each data point represents an individual focus. Horizontal red bar indicates the median. F) The percentage of total recruitment regions in PMT that were either clusters (>0.6 μm, black) or foci (≤0.6 μm, gray). G) Number of recruitment regions per nucleus in MP. H) Time of focus appearance (minutes) in microirradiated nuclei of MP. Each data point represents an individual focus. Horizontal red bar indicates the median. I) The percentage of total recruitment regions in MP that were either clusters (>0.6 μm, black) or foci (≤0.6 μm, gray). J) A representative image of microirradiation-induced damage marked by MRE-11 next to the SC, here stained by the axial element HTP-3 (red). The two HTP-3 parallel stacks are from 2 different chromosomes, one containing MRE-11 cluster (arrow) and one not. Cartoon representation on the far right used the same colors as seen in the staining, except chromosomes that are not microirradiated are in yellow. Only the DNA of the microirradiated chromosome is represented in the cartoon (standard chromatin loop model). Kruskal-Wallis was applied to determine significant differences between rank means in C, D, E, G, and H, and if there was determination of significant differences Mann-Whitney U-test was applied for each pairwise comparison. Fisher's Exact Test (two-tailed) was applied for all pairwise comparisons in B, F, and I.

points and remained around 2–2.5 foci per nucleus for the remainder of the time course, potentially indicating that there is a maximum number of separate foci that will form (Fig. 4D). The number of clusters per nucleus (2.1), the number of foci per cluster (4.1), and the area of each cluster (0.48 μm^2) is significantly higher at 24 h post-microirradiation compared to all other time points analyzed (Figs. 4E, F, and S3A). These data indicate that the significant increase in total foci between immediate and 1 h time points is largely due to the appearance of separate foci, while the significant increase at 2–24 hours is largely due to expansion of foci number within clusters. The percentage of foci versus clusters reflects this trend as well, as there are significantly more foci than clusters in the 1- and 2 -h time points with respect to the 24 -h time point (Fig. 3B). However, the total number of recruitment regions of DNA damage do not significantly increase after the 1 -h time point (2.2 and 3.8 in immediate vs. 1 h; Fig. 4G). This could potentially mean that all sites of DNA damage have recruited MRE-11 to the point of detection by the 1 -h time point, and that following 1 h, half of these sites continue to accumulate more MRE-11 over time. While some nuclei have clusters that exhibit expansion over time, the overall number of nuclei with foci decreases significantly by the 24 -h time point, with a decrease from ~75 % of nuclei targeted with microirradiation showing MRE-11 foci at the immediate to 2 -h time points versus only ~50 % of targeted nuclei with MRE-11 foci at 24 h (Fig. 4H). This suggests that cluster expansion occurs in cells in which DSB repair is delayed or fails.

Next, we examined what drives cluster expansion. Since nuclei move in the germline as time progresses, it is possible that the expansion of foci numbers from 2–24 hours is due to their movement from TZ to MP (stage in meiosis) and not due to the progression of repair (time). If the meiotic stage determines expansion, then microirradiation of nuclei in MP should lead to immediate cluster expansion (Fig. S3). However, the

number of foci per nuclei following microirradiation was similar in TZ and MP immediate time points and grow in similar proportion. Examining the structure of clusters at 24 h post-microirradiation of MP nuclei was not attainable since these nuclei would have progressed to diakinesis. The overall number of foci per nucleus was higher in MP versus TZ, consistent with our live imaging data (Fig. 1C). Accumulation of MRE-11 foci within a cluster can be an outcome of recruitment of MRE-11 separate foci to an existing focus/cluster or expansion of a cluster. To test this, we performed hour-long imaging of live worms (40 s intervals to avoid bleaching). We observed no evidence for foci recruitment to clusters/foci convergence via live imaging (Fig. S4, Movie S2). Altogether, this suggests that clusters increase foci numbers by measure of expansion, likely as a function of their progression in the process of DNA damage repair.

3.5. Proteins from HR and NHEJ repair pathways show recruitment to, and colocalization at, microirradiation-induced DSBs

There is no evidence for the involvement of NHEJ in the repair of SPO-11 or γ-IR induced breaks in the wild-type *C. elegans* germline. Indeed, KU-80 (a member of the KU complex) foci are not apparent on SPO-11 nor on γ-IR induced DSBs (Figs. 5A and S5B). In the same conditions RAD-51 can be recruited to foci (Fig. 5B, S5B). This is consistent with the genetic evidence suggesting that DSB repair in the wild-type germline is committed to HR [19,39,40]. However, it is formally possible that other types of DSBs can recruit NHEJ proteins. We have shown that microirradiation induces clustered DSBs (Fig. 4). We therefore tested the hypothesis that clustered DSBs are capable of recruiting NHEJ proteins (methodology in Fig. 5CD). We found that in complete contrast to what is found for SPO-11 and γ-IR induced breaks, cKU-80 is recruited to microirradiation-induced breaks, and that it does show some colocalization with MRE-11, mostly on clusters (Fig. 5EH and S5C). Although this was not demonstrated in *C. elegans*, it is possible that this colocalization indicates MRN activity in NHEJ. However, RAD-51, an obligatory HR protein, also colocalized with cKU-80 as well within clusters (Fig. 5FI and S5D). Unlike MRE-11, RAD-51 activity is not found in any NHEJ pathway, thus this colocalization indicates that HR and NHEJ proteins can be found at the same sites of complex DNA damage. We then examined colocalization between two HR proteins that act in different steps of repair: MRE-11 and RAD-51. As we found above for other proteins, MRE-11 colocalized with RAD-51 in a fraction of cases, and clusters of both MRE-11 and RAD-51 exhibited more colocalization than did individual foci (Figs. 5GJ and S5E). This is consistent with MRE-11 being maintained at the break following resection. In all cases examined, separate foci are mainly found at a distance (far, Fig. S5F-K). To conclude, this suggests that clusters represent many breaks in one location that may be undergoing different forms of repair and that clustered DSBs use mixed HR/NHEJ repair for different breaks within a cluster. One caveat of using microirradiation to produce DNA damage is that the location of the DSBs is random, thus the outcome of the repair process cannot be assessed.

3.6. Deletion of cKU-70 inhibits the formation of MRE-11 clusters in mitotic and early meiotic regions

With evidence that both NHEJ and HR factors are recruited to the DSB clusters induced by microirradiation, we wanted to determine whether recruitment of MRE-11 would be affected by the presence of a functional NHEJ pathway. The kinetics of MRE-11 recruitment were largely unaffected by the deletion of cKU-70 (Figs. 6A–D and S6A–D), with a slight increase in the amount of time it takes for MRE-11 to appear in TZ (1.8–2.5 minutes Fig. 6SB) and an increase in the number of MRE-11 recruitment regions formed in LP (1–2.3 Fig. 6D). The latter may indicate an inhibitory role for KU on MRE-11 recruitment in LP. The most notable difference observed with deletion of cKU-70 was the change in the percent of clusters and foci in PMT and TZ (Fig. 6E–H). In a *cku-70* background, MRE-11 forms significantly fewer clusters in PMT (37 % to 10 %, Fig. 6E) and TZ (47 % to 10 %, Fig. 6F), whereas the relative proportion of clusters and foci was unchanged in MP and LP (Fig. 6G and H). Since the overall number of foci is not increased in PMT, TZ, and MP (Fig. 6A-C), these changes cannot be attributed to clusters breaking apart to individual foci, but to a lower level of MRE-11 on clusters that may lead to their classification as foci. Lower recruitment levels to clusters may also explain the increase in recruitment time in TZ (Fig. S6B).

MRE-11 is required for resection of SPO-11 and γ-irradiation-induced DSBs in meiosis [19,27] and this resection is evidenced by formation of RAD-51 foci [19]. Following microirradiation in TZ neither the number of RAD-51 foci per nucleus nor the ratio of RAD-51 foci to MRE-11 foci changed with abrogation of cKU-70 (Fig. S6E and F). This is also reflected in the levels of colocalization of MRE-11 with RAD-51, which are similar between the two strains and show a similar pattern of colocalization being largely in clusters, as seen in Fig. 5 (Fig. S6G and H). This indicates that the attenuated recruitment of MRE-11 is sufficient to promote resection (leading to RAD-51 focus formation) at clustered DSB damage sites.

3.7. Deletion of COM-1 inhibits the recruitment and nucleolytic activity of MRE-11 in mid- to late-pachytene

MRN activity at SPO-11 breaks is dependent on COM-1/CtIP, its catalytic obligatory co-factor in meiosis [41]. Indeed, *com-1* null mutants are phenotypically indistinguishable from *mre-11* catalytically null mutants [19,42]. Since MRE-11 is thought to be recruited to DSBs as part of a complex with SPO-11, COM-1, which does not play a role in DSB formation, is considered irrelevant to MRE-11 recruitment to DSB sites. However, microirradiation produces DSBs with no covalently bound proteins at the ends. This raises the possibility that COM-1 would play a different role in recruitment and activity of MRE-11 at this form of damage. The previously described *com-1(t1626)* mutant was linked to a mutation that affected gonad length (*unc-32*), which complicates the comparable analysis to our other data performed in a wild-type germline structure. Therefore, we generated a deletion mutant of *com-1* (*com-1 (iow101)*) via CRISPR/Cas9 in an otherwise wild-type strain. *com-1 (iow101)* contains an out-of-frame deletion which removes 94 % of the last exon (the most conserved region of COM-1), has a range of 1–12 DAPI bodies in diakinesis, and is homozygous sterile, all similar phenotypes to other COM-1 mutants that have been generated [42].

COM-1 deletion did not have an effect on the timing of MRE-11 appearance in any of the germline regions (Fig. S7A–D). However, there were significantly fewer MRE-11 recruitment regions that appeared in both MP (2.1 to 0.9) and LP (1.4 to 0.5), compared to other stages (Fig. 7A–D). Unlike what was found for *cku-70*, the ratio of clusters to foci was unchanged in all zones (Fig. S7E–H). The significant change in the number of MRE-11 foci being recruited to microirradiation damage in MP and LP led us to test whether or not the activity of MRE-11 was similarly reduced in these zones, as COM-1 in other organisms is shown to promote the nucleolytic activity of MRE-11. As a control, we also assayed the effect of COM-1 deletion on MRE-11 activity in TZ, a zone in which we saw no change in MRE-11 recruitment in our live-imaging assay. When microirradiated at TZ, no change in the levels of MRE-11 recruitment was observed in terms of number of RAD-51 foci generated or in the ratio of RAD-51 to MRE-11 foci (Fig. 7E and F). However, when the same experiment was performed in MP, significantly fewer RAD-51 foci were formed compared to the wild-type background (12 to 7 RAD-51 foci/nucleus, Fig. 7G). Similar results were obtained at the immediate time point (12 min: 4 to 2 RAD-51 foci per nucleus, Fig. 7G). The ratio of RAD-51 to MRE-11 was similarly reduced at both time points for MP in the *com-1* deletion mutants (Fig. 7H). The ratio of foci/clusters or colocalization of MRE-11 with RAD-51 was similar to wild type in both zones assayed (Fig. S7E-K). Together, these data indicate that COM-1 enhances the recruitment and thus the nucleolytic

activity of MRE-11 at complex DNA damage in pachytene.

3.8. The SC affects the recruitment of MRE-11 to microirradiation-induced DSBs

The SC is a meiosis-specific complex that assembles between homologous chromosomes to target DSB repair to the homologous chromosome (as opposed to the sister chromatid) through the HR pathway. In *C. elegans,* the SC is assembled independently from DSB formation and has minimal effects on meiotic chromosome movement [43,44]. In the germline, the SC begins assembly in TZ, is fully formed in MP, and begins to disassemble at late LP [45]. The microirradiation performed at LP was in the nuclei just prior to SC disassembly. For both c*ku-70* and *com-1* mutants we saw effects that are different between pachytene regions and PMT/TZ. Therefore we hypothesized that the SC plays a role in regulating cluster cohesion and/or MRE-11 recruitment. To test this, we removed the SC using a *syp-3* mutant in the absence or presence of *cku-70* or *com-1*. *syp-3* encodes a structural protein of the SC [46]. Importantly, SYP-3 is a central region protein of the SC and as such acts downstream of DSB formation or sister chromatid cohesion [46,47].

First, we tested whether the SC plays a role in enabling or facilitating the formation of larger foci on clustered DSBs in the absence of *cku-70*. *syp-3* mutants had no effect on timing of MRE-11 recruitment or formation of clustered DSBs (Fig. 8B and C). However, simultaneous deletion of both *syp-3* and *cku-70*, while not changing the number of foci (Fig. S8A) led to a significant reduction in the relative proportion of clusters to foci in mid-pachytene (from 44 % to 23 % clusters, Fig. 8B) and increase in their time of appearance (Fig. 8C). This suggests that both the SC and cKU-70 affect cluster cohesion.

We have shown that COM-1 is aiding MRE-11 recruitment to, and function at, complex DSBs induced in the context of a fully formed SC (Fig. 7). To test if the SC inhibits MRE-11 recruitment in the absence of COM-1, we tested MRE-11::GFP focus formation in *com-1*; *syp-3* double mutants. Microirradiation in PMT where no SC is formed, has no effect on MRE-11 recruitment in *com-1; syp-3* compared to *com-1* mutant (Fig. 8D-F). However, in a zone with fully assembled SC, deletion of *syp-3* suppressed the recruitment defects found in *com-1* mutant (Fig. 8G), without affecting other parameters tested (Fig. 8H and I). Similar effects were observed when *him-3*, an axial component of the SC, was removed (Fig. S8B-G) [48]. Since *him-3* and *syp-3* mutants have opposing effects on chromosomal nuclear positioning, we conclude that effects we see on MRE-11 recruitment are likely direct [46,48]. Overall, our data suggests that COM-1 is required to stabilize the MRN complex in order to access damage, and that this function is important in the context of a fully formed SC.

The effect of the SC on MRE-11 suggested that the SC is present in proximity to the MRE-11 recruitment regions. However, studies of γ-irradiation have shown that the SC can disassemble in response to DNA damage, which results in bifurcation of the SC axis [49]. We did not observe such disassembly following microirradiation at similar conditions (n = 31). This indicates the SC maintains its structural role next to clustered DSB sites (Fig. 8J).

4. Discussion

The germline is a tissue in which programmed DSBs are committed to repair by HR. Exogenously-induced DSBs in meiosis can be repaired by HR, creating DSBs that can substitute for SPO-11-induced breaks, but may be also be repaired by other pathways. Here we have shown that clustered DSBs may impose a different DSB repair pathway choice decision on meiotic nuclei that now recruit HR and NHEJ proteins. Although recruitment of repair proteins to the break is suggestive of repair pathway activation, in the absence of an assay for the repair outcome of microirradiation-induced DSBs this cannot be directly tested. However, recruitment of repair proteins to the break site is an essential step required for pathway utilization and thus is informative. Our studies suggest that recruitment of DSB repair proteins to breaks can be a mode of regulation of their activity.

4.1. Repair of clustered DSBs in the germline involves the recruitment of HR and NHEJ proteins

Ionizing radiation induces DNA damage in the form of nicks that, when found adjacent to each other, form DSBs [25]. This mechanism is common to all forms of ionizing radiation including heavy particle radiation used in cancer therapy, γ-irradiation, and microirradiation [50]. Since nicks can be easily repaired, they are not considered mutagenic. However, DSBs are more deleterious and require repair prior to cell division. Different forms of radiation differ in the relative abundance of clustered DSBs, with high LET exposure (heavy ion) producing more clustered DSBs than low LET exposure (γ-irradiation). In agreement with studies from tissue culture, we show that microirradiation produces clusters of DSBs in the germline of intact organisms ([21] and this paper). This supports microirradiation as an effective method for the study of clustered DSBs.

Studies in tissue culture indicate that the repair of clustered DSBs does not follow the normal repair program. Cells that typically engage in DSB repair via NHEJ shift their repair pathway choice to a mixed HR/NHEJ model [2]. In mammalian tissue culture studies NHEJ factors such as the KU complex accumulate at microirradiation-induced DNA damage, and whether or not the break undergoes NHEJ or HR, both pathways' repair factors are often present [51–53]. In the germline, DSBs are committed to repair via HR and we have shown that DSB clusters still recruit HR proteins ([21] and this paper). Because in tissue culture NHEJ shifts to an NHEJ/HR model, this may imply that HR is the preferred pathway for repair of clustered DSBs [2]. In the germline, we discovered that both NHEJ and HR proteins are recruited to microirradiation-induced breaks, regardless of the fact that repair of SPO-11-induced breaks is committed to HR. This suggests that clustered DSBs are a special form of DNA damage that may create a unique repair environment compared to when the same amount of damage is dispersed throughout the genome.

The colocalization of RAD-51 and cKU-80 at clusters but not at foci indicates that HR and NHEJ events target the same cluster. The requirement for multiple repair pathways may stem from the combination of different types of substrates at the break. Assuming a random positioning of nicks caused by microirradiation, it is likely that some will contain substrates favorable for c-NHEJ (blunt or almost blunt ends), while others can be targeted to MMEJ (short ssDNA overhangs) or HR (long ssDNA overhangs). The colocalization of HR and NHEJ proteins on a single focus in a cluster may reflect these two pathways in the process of competition on processing a break. Clustered DSBs also create new repair substrates-short pieces of dsDNA-that may be especially challenging to repair and thus attempt repair by several pathways [54].

4.2. MRE-11 dynamics at complex DNA damage sites

MRE-11 is one of the first proteins recruited to exogenously-induced DNA damage in mammalian tissue culture cells, forming foci within the first few minutes [35,36,55]. Our studies identified similar kinetics in *C. elegans* germline nuclei, showing a remarkable evolutionary conservation of this trait in metazoans. The time by which most MRE-11 foci are appearing precedes that of RPA-1 and RAD-51 foci [21] in agreement with the role of MRN(X) in DSB resection. Here we have shown that MRE-11 kinetics at the sites of DSBs can be unique to different germline regions (Fig. 1) or altered in mutants (Figs. 6–8). Since these changes do not affect the level of DNA damage, the changes in recruitment of MRE-11 reflects change in its regulation.

One of the interesting findings we discovered is the growth in cluster size over time, likely due to expansion (Fig. S4, Movie S2). The most significant cluster expansion (Fig. 4F) occurs after about a third of MRE-11 recruitment regions disappeared (Fig. 4H), suggesting that cluster

expansion occurs at regions that are harder to repair. Cluster expansion could be an indication of ongoing repair and may be attributed to chromatin relaxation or a conversion of local damage into substrates that are suitable for MRE-11 recruitment over time.

4.3. KU at complex DNA damage

Following microirradiation, KU is found in both foci and clusters. The fact that KU is recruited to foci formed by microirradiation but not by SPO-11 or γ-irradiation suggests that clustered DSBs engage with the NHEJ pathway in the germline. With the tools we currently have we do not know if recruitment of NHEJ proteins actually means repair. Although cKU is recruited to microirradiation-induced breaks, it has a relatively small effect on MRE-11's recruitment and mostly affects the ability of MRE-11 to accumulate on more complex repair sites (clusters). DSB clusters may be more susceptible to structural damage, as they contain short dsDNA fragments, and it is possible that KU's action is required to maintain the integrity of the cluster in a way that facilitates protein recruitment throughout the cluster. The synergistic effect of *syp-3* and *cku-70* mutants may support such a model, as SYP-3 is part of a complex with structural function on meiotic chromosomes.

4.4. COM-1 at complex DNA damage

COM-1/Sae2/CtIP is an MRN(X) co-factor, promoting the resection activity of MRE-11 at the site of DSBs [8,42,56]. COM-1 homologues have other more controversial roles; having their own endonuclease activity and/or DNA bridging functions. COM-1's activity as an MRN co-factor may be executed via various mechanisms and here we show that one of them may be the recruitment of MRE-11 to DSBs (Fig. 7), which as a consequence, can promote its resection activity (Fig. 7F and H). Microirradiation-induced breaks are likely available for all nucleases (not blocked by SPO-11), thus RAD-51 focus formation is not completely dependent on COM-1. SC removal suppresses the defects found in *com-1* mutants in MP but not PMT nuclei (Fig. 8), which suggests that the presence of the SC is an inhibiting factor for MRE-11 recruitment and is overcome by COM-1's action in stabilization of the MRN complex. In agreement, in yeast a mutant in the SC axial component Red1, partially rescued the meiotic defect seen in *com1/sae2* mutants [57].

Altogether these results show that MRE-11 recruitment to clustered DSBs can be modulated throughout meiotic prophase I, and by alterations in other DNA repair pathways and accessory proteins. The damage induced by microirradiation in wild-type germ cells can recruit NHEJ pathway proteins. This presents a complex nature of regulation of pathway choice at clustered DSBs in a meiotic context.

Author statement

Kailey Harrell: Conceptualization; Data curation; Investigation; Formal analysis; Investigation; Resources; Methodology; Supervision; Validation; Visualization; Roles/Writing - original draft; Writing - review & editing.

Madison Day: Investigation; Writing – review & editing.

Sarit Smolikove: Conceptualization; Funding acquisition; Methodology; Project administration; Resources; Supervision; Validation; Visualization; Writing - review & editing.

Funding source

R01GM112657 To Sarit Smolikove.

Transparency document

The Transparency document associated with this article can be found in the online version.

Declaration of Competing Interest

The authors declare that there are no conflicts of interest.

Acknowledgements

Some strains and clones were kindly provided by the *Caenorhabditis* Genetics Center, which is funded by the National Institutes of Health Office of Research Infrastructure Programs (P40 OD-010440), and the *C. elegans* Reverse Genetics Core Facility at the University of British Columbia, which is part of the International *C. elegans* Gene Knockout Consortium. We acknowledge the staff at the University of Iowa College of Medicine and Holden Comprehensive Cancer Center Radiation and Free Radical Research (RFRR) Core for radiation services. The RFRR core facility is supported by funding from NIH P30 CA086862. We would like to thank Dylan Cooke, Emily Koury, and Richard Bowman for their help with experiments. We thank all members of the Smolikove lab and A. Malkova for their critical reading of this manuscript. This work was funded by NIH grant number R01GM112657 (to S.S.).

Appendix A. Supplementary data

Supplementary material related to this article can be found, in the online version, at doi:https://doi.org/10.1016/j.mrfmmm.2021.111743.

References

[1] V. Sharma, L.B. Collins, T.-H. Chen, N. Herr, S. Takeda, W. Sun, J.A. Swenberg, J. Nakamura, Oxidative stress at low levels can induce clustered DNA lesions leading to NHEJ mediated mutations, Oncotarget 7 (2016) 25377–25390.
[2] H. Wang, X. Zhang, P. Wang, X. Yu, J. Essers, D. Chen, R. Kanaar, S. Takeda, Y. Wang, Characteristics of DNA-binding proteins determine the biological sensitivity to high-linear energy transfer radiation, Nucleic Acids Res. 38 (2010) 3245–3251.
[3] S. Keeney, C.N. Giroux, N. Kleckner, Meiosis-specific DNA double-strand breaks are catalyzed by Spo11, a member of a widely conserved protein family, Cell 88 (1997) 375–384.
[4] G. Hamer, H. Wang, E. Bolcun-Filas, H.J. Cooke, R. Benavente, C. Höög, Progression of meiotic recombination requires structural maturation of the central element of the synaptonemal complex, J. Cell. Sci. 121 (2008) 2445–2451.
[5] S.L. Page, R.S. Hawley, The genetics and molecular biology of the synaptonemal complex, Annu. Rev. Cell Dev. Biol. 20 (2004) 525–558.
[6] E. Hartsuiker, K. Mizuno, M. Molnar, J. Kohli, K. Ohta, A.M. Carr, Ctp1CtIP and Rad32Mre11 nuclease activity are required for Rec12Spo11 removal, but Rec12Spo11 removal is dispensable for other MRN-dependent meiotic functions, Mol. Cell. Biol. 29 (2009) 1671–1681.
[7] E.P. Mimitou, L.S. Symington, Sae2, Exo1 and Sgs1 collaborate in DNA double-strand break processing, Nature 455 (2008) 770–774.
[8] E. Cannavo, P. Cejka, Sae2 promotes dsDNA endonuclease activity within Mre11-Rad50-Xrs2 to resect DNA breaks, Nature 514 (2014) 122–125.
[9] R. Anand, L. Ranjha, E. Cannavo, P. Cejka, Phosphorylated CtIP functions as a Co-factor of the MRE11-RAD50-NBS1 endonuclease in DNA end resection, Mol. Cell 64 (2016) 940–950.
[10] X. Wang, J.E. Haber, Role of Saccharomyces Single-Stranded DNA-Binding protein RPA in the strand invasion step of double-strand break repair, PLoS Biol. 2 (2004) e21.
[11] L.F. Povirk, Processing of damaged DNA ends for double-strand break repair in mammalian cells, ISRN Mol. Biol. 2012 (2012).
[12] M.R. Lieber, Y. Ma, U. Pannicke, K. Schwarz, Mechanism and regulation of human non-homologous DNA end-joining, Nature reviews, Mol. Cell Biol. 4 (2003) 712–720.
[13] E.A. Ahmed, A. Sfeir, H. Takai, H. Scherthan, Ku70 and non-homologous end joining protect testicular cells from DNA damage, J. Cell. Sci. 126 (2013) 3095.
[14] I. Clejan, J. Boerckel, S. Ahmed, Developmental modulation of nonhomologous end joining in Caenorhabditis elegans, Genetics 173 (2006) 1301–1317.
[15] E.F. Joyce, A. Paul, K.E. Chen, N. Tanneti, K.S. McKim, Multiple barriers to nonhomologous DNA end joining during meiosis in Drosophila, Genetics 191 (2012) 739–746.
[16] W. Goedecke, M. Eijpe, H.H. Offenberg, M. van Aalderen, C. Heyting, Mre11 and Ku70 interact in somatic cells, but are differentially expressed in early meiosis, Nat. Genet. 23 (1999) 194–198.
[17] S.E. Lee, F. Paques, J. Sylvan, J.E. Haber, Role of yeast SIR genes and mating type in directing DNA double-strand breaks to homologous and non-homologous repair paths, Curr. Biol. 9 (1999) 767–770.

[18] M. Valencia, M. Bentele, M.B. Vaze, G. Herrmann, E. Kraus, S.E. Lee, P. Schar, J. E. Haber, NEJ1 controls non-homologous end joining in Saccharomyces cerevisiae, Nature 414 (2001) 666–669.
[19] Y. Yin, S. Smolikove, Impaired resection of meiotic double-strand breaks channels repair to nonhomologous end joining in Caenorhabditis elegans, Mol. Cell. Biol. 33 (2013) 2732–2747.
[20] H. Yun, K. Kim, Ku complex suppresses recombination in the absence of MRX activity during budding yeast meiosis, BMB Rep. 52 (2019) 607–612.
[21] E. Koury, K. Harrell, S. Smolikove, Differential RPA-1 and RAD-51 recruitment in vivo throughout the C. Elegans germline, as revealed by laser microirradiation, Nucleic Acids Res. 46 (2018) 748–764.
[22] E.P. Rogakou, C. Boon, C. Redon, W.M. Bonner, Megabase chromatin domains involved in DNA double-strand breaks in vivo, J. Cell Biol. 146 (1999) 905–916.
[23] C. Lukas, F. Melander, M. Stucki, J. Falck, S. Bekker-Jensen, M. Goldberg, Y. Lerenthal, S.P. Jackson, J. Bartek, J. Lukas, Mdc1 couples DNA double-strand break recognition by Nbs1 with its H2AX-dependent chromatin retention, EMBO J. 23 (2004) 2674–2683.
[24] V. Popuri, M. Ramamoorthy, T. Tadokoro, D.K. Singh, P. Karmakar, D.L. Croteau, V.A. Bohr, Recruitment and retention dynamics of RECQL5 at DNA double strand break sites, DNA Repair (Amst.) 11 (2012) 624–635.
[25] L. Lan, S. Nakajima, Y. Oohata, M. Takao, S. Okano, M. Masutani, S.H. Wilson, A. Yasui, In situ analysis of repair processes for oxidative DNA damage in mammalian cells, Proc. Natl. Acad. Sci. U. S. A. 101 (2004) 13738–13743.
[26] X. Kong, S.K. Mohanty, J. Stephens, J.T. Heale, V. Gomez-Godinez, L.Z. Shi, J. S. Kim, K. Yokomori, M.W. Berns, Comparative analysis of different laser systems to study cellular responses to DNA damage in mammalian cells, Nucleic Acids Res. 37 (2009) e68.
[27] G.M. Chin, A.M. Villeneuve, C. elegans mre-11 is required for meiotic recombination and DNA repair but is dispensable for the meiotic G(2) DNA damage checkpoint, Genes Dev. 15 (2001) 522–534.
[28] K.E. Harrell, E. Koury, S. Smolikove, Microirradiation for precise, double-strand break induction in vivo in Caenorhabditis elegans, Bio-Protocol 8 (2018).
[29] J.-Y. Tinevez, N. Perry, J. Schindelin, G.M. Hoopes, G.D. Reynolds, E. Laplantine, S. Y. Bednarek, S.L. Shorte, K.W. Eliceiri, TrackMate: An open and extensible platform for single-particle tracking, Methods (San Diego, Calif.) 115 (2017) 80–90.
[30] S. Pauklin, J.S. Burkert, J. Martin, F. Osman, S. Weller, S.J. Boulton, M.C. Whitby, S.K. Petersen-Mahrt, Alternative induction of meiotic recombination from single-base lesions of DNA deaminases, Genetics 182 (2009) 41–54.
[31] A. Hefel, M. Honda, N. Cronin, K. Harrell, P. Patel, M. Spies, S. Smolikove, RPA complexes in Caenorhabditis elegans meiosis; unique roles in replication, meiotic recombination and apoptosis, Nucleic Acids Res. (2021).
[32] E.P. Mimitou, L.S. Symington, DNA end resection: many nucleases make light work, DNA Repair 8 (2009) 983–995.
[33] H. Ogawa, K. Johzuka, T. Nakagawa, S.H. Leem, A.H. Hagihara, Functions of the yeast meiotic recombination genes, MRE11 and MRE2, Adv. Biophys. 31 (1995) 67–76.
[34] R. Reichman, Z. Shi, R. Malone, S. Smolikove, Mitotic and meiotic functions for the SUMOylation pathway in the Caenorhabditis elegans germline, Genetics 208 (2018) 1421–1441.
[35] A.N. Suhasini, J.A. Sommers, P.A. Muniandy, Y. Coulombe, S.B. Cantor, J. Y. Masson, M.M. Seidman, R.M. Brosh Jr., Fanconi anemia group J helicase and MRE11 nuclease interact to facilitate the DNA damage response, Mol. Cell. Biol. 33 (2013) 2212–2227.
[36] R.A. Shamanna, H. Lu, J.K. de Freitas, J. Tian, D.L. Croteau, V.A. Bohr, WRN regulates pathway choice between classical and alternative non-homologous end joining, Nat. Commun. 7 (2016) 13785.
[37] M. Kressel, P. Groscurth, Distinction of apoptotic and necrotic cell death by in situ labelling of fragmented DNA, Cell Tissue Res. 278 (1994) 549–556.
[38] A. Alpi, P. Pasierbek, A. Gartner, J. Loidl, Genetic and cytological characterization of the recombination protein RAD-51 in Caenorhabditis elegans, Chromosoma 112 (2003) 6–16.
[39] B.B. Lemmens, N.M. Johnson, M. Tijsterman, COM-1 promotes homologous recombination during Caenorhabditis elegans meiosis by antagonizing Ku-mediated non-homologous end joining, PLoS Genet. 9 (2013), e1003276.
[40] C. Girard, B. Roelens, K.A. Zawadzki, A.M. Villeneuve, Interdependent and separable functions of *Caenorhabditis elegans* MRN-C complex members couple formation and repair of meiotic DSBs, Proc. Natl. Acad. Sci. (2018).
[41] A.H. McKee, N. Kleckner, A general method for identifying recessive diploid-specific mutations in Saccharomyces cerevisiae, its application to the isolation of mutants blocked at intermediate stages of meiotic prophase and characterization of a new gene SAE2, Genetics 146 (1997) 797–816.
[42] A. Penkner, Z. Portik-Dobos, L. Tang, R. Schnabel, M. Novatchkova, V. Jantsch, J. Loidl, A conserved function for a Caenorhabditis elegans Com1/Sae2/CtIP protein homolog in meiotic recombination, EMBO J. 26 (2007) 5071–5082.
[43] A.F. Dernburg, K. McDonald, G. Moulder, R. Barstead, M. Dresser, A.M. Villeneuve, Meiotic recombination in C. Elegans initiates by a conserved mechanism and is dispensable for homologous chromosome synapsis, Cell 94 (1998) 387–398.
[44] A. Baudrimont, A. Penkner, A. Woglar, T. Machacek, C. Wegrostek, J. Gloggnitzer, A. Fridkin, F. Klein, Y. Gruenbaum, P. Pasierbek, V. Jantsch, Leptotene/Zygotene chromosome movement via the SUN/KASH protein bridge in Caenorhabditis elegans, PLoS Genet. 6 (2010), e1001219.
[45] K. Nabeshima, A.M. Villeneuve, M.P. Colaiácovo, Crossing over is coupled to late meiotic prophase bivalent differentiation through asymmetric disassembly of the SC, J. Cell Biol. 168 (2005) 683–689.
[46] S. Smolikov, A. Eizinger, K. Schild-Prufert, A. Hurlburt, K. McDonald, J. Engebrecht, A.M. Villeneuve, M.P. Colaiácovo, SYP-3 restricts synaptonemal complex assembly to bridge paired chromosome axes during meiosis in Caenorhabditis elegans, Genetics 176 (2007) 2015–2025.
[47] D.Y. Lui, M.P. Colaiácovo, Meiotic development in Caenorhabditis elegans, Adv. Exp. Med. Biol. 757 (2013) 133–170.
[48] M.C. Zetka, I. Kawasaki, S. Strome, F. Müller, Synapsis and chiasma formation in Caenorhabditis elegans require HIM-3, a meiotic chromosome core component that functions in chromosome segregation, Genes Dev. 13 (1999) 2258–2270.
[49] F. Couteau, M. Zetka, DNA damage during meiosis induces chromatin remodeling and synaptonemal complex disassembly, Dev. Cell 20 (2011) 353–363.
[50] J.A. Nickoloff, N. Sharma, L. Taylor, Clustered DNA double-strand breaks: biological effects and relevance to cancer radiotherapy, Genes (Basel) 11 (2020) 99.
[51] P.-O. Mari, B.I. Florea, S.P. Persengiev, N.S. Verkaik, H.T. Brüggenwirth, M. Modesti, G. Giglia-Mari, K. Bezstarosti, J.A.A. Demmers, T.M. Luider, A. B. Houtsmuller, D.C. Van Gent, Dynamic assembly of end-joining complexes requires interaction between Ku70/80 and XRCC4, Proc. Natl. Acad. Sci. U. S. A. 103 (2006) 18597–18602.
[52] B. Muster, A. Rapp, M.C. Cardoso, Systematic analysis of DNA damage induction and DNA repair pathway activation by continuous wave visible light laser microirradiation, AIMS Genet. 4 (2017) 47–68.
[53] R. Aleksandrov, A. Dotchev, I. Poser, D. Krastev, G. Georgiev, G. Panova, Y. Babukov, G. Danovski, T. Dyankova, L. Hubatsch, A. Ivanova, A. Atemin, M. N. Nedelcheva-Veleva, S. Hasse, M. Sarov, F. Buchholz, A.A. Hyman, S.W. Grill, S. S. Stoynov, Protein dynamics in complex DNA lesions, Mol. Cell 69 (2018) 1046–1061, e1045.
[54] D. Pang, T.A. Winters, M. Jung, S. Purkayastha, L.R. Cavalli, S. Chasovkikh, B. R. Haddad, A. Dritschilo, Radiation-generated short DNA fragments may perturb non-homologous end-joining and induce genomic instability, J. Radiat. Res. 52 (2011) 309–319.
[55] J.S. Kim, T.B. Krasieva, H. Kurumizaka, D.J. Chen, A.M. Taylor, K. Yokomori, Independent and sequential recruitment of NHEJ and HR factors to DNA damage sites in mammalian cells, J. Cell Biol. 170 (2005) 341–347.
[56] M. Clerici, D. Mantiero, G. Lucchini, M.P. Longhese, The Saccharomyces cerevisiae Sae2 protein promotes resection and bridging of double strand break ends, J. Biol. Chem. 280 (2005) 38631–38638.
[57] D. Woltering, B. Baumgartner, S. Bagchi, B. Larkin, J. Loidl, T. de los Santos, N. M. Hollingsworth, Meiotic segregation, synapsis, and recombination checkpoint functions require physical interaction between the chromosomal proteins Red1p and Hop1p, Mol. Cell. Biol. 20 (2000) 6646–6658.